Chapter 9

Magnetization Statics and Ultrafast Photoinduced Dynamics in Co/garnet Heterostructures

Andrzej Stupakiewicz

Additional information is available at the end of the chapter

http://dx.doi.org/10.5772/62542

Abstract

We demonstrate experimental studies of the magnetization behavior from statics to ultrafast photoinduced dynamics with high temporal resolution in ultrathin Co/garnet heterostructures with a sub-nanometer roughness at the interface. We report on modulation of spin precession in Co/garnet heterostructures with distinct frequencies and show that the excitation efficiency of these precessions strongly depends on the amplitude and the direction of external magnetic field. Furthermore, it is shown that the magnetization precession in the garnet film can be manipulated by the strong magnetostatic coupling between Co and garnet layers. These findings could provide new possibilities in all-optical excitation and local spin manipulation by polarized femtosecond pulses for the application in nanodevices with high-speed switching.

Keywords: ultrafast magnetization dynamics, magneto-optical effect, magnetization reversal, magnetic anisotropy, magnetic domain structure, photomagnetism, ferromagnetic resonance, garnet, cobalt

1. Introduction

Control of magnetization with the help of femtosecond laser pulses is a hot topic in fundamental science [1–5]. Understanding ultrafast magnetization dynamics on an ultrashort timescale promises to enable technologies based on the quantum-level interplay of nonlinear optics and magnetism. All-optical control of the magnetism in novel magnetic materials is a particularly important issue for further development of faster magnetic information storage/processing and spintronic nanodevices. The thermal effect limits the application of the technology of heat-assisted magnetic recording due to relatively long cooling time (~1 ns) [6]. One of the solu-

tions to this problem can be all-optical nonthermal control of the magnetization. For fundamental research, hybrid structures give the unique possibility to engineer high-quality two-dimensional interfaces and create phenomena which do not exist in a bulk material. On the contrary, new functionalities may emerge from the coexistence of two materials with complementary properties, such as magnetism and ferroelectricity, metallic and dielectric, antiferromagnetic and ferromagnetic, etc.

An interesting combination is formed by a metallic ferromagnetic ultrathin film on top of a dielectric ferrimagnet, based on yttrium iron garnet (YIG) with different substitutions. The functionality of YIG systems has been shown to be very broad, with examples such as the excitation of surface plasmons [7], the propagation of nonlinear spin-waves [8, 9], Bose-Einstein condensation of a magnon gas [10], high-temperature photomagnetism [11], the observation of the inverse Faraday effect induced by an ultrafast laser pulse [12–14], and many others. A combination of a metal layer on a garnet system may create the possibility to modify different properties. Recently, it was reported that ion beam sputtered Fe films on a 100 nm-thick YIG layer possess a perpendicular magnetic anisotropy [15]. In the thickness range between 5 and 10 nm, the stripe domain structure of YIG was transferred into the Fe films due to the presence of strong interlayer exchange coupling [15]. Static and dynamic properties were also investigated for a 30-nm permalloy film on a 0.5 μm $(YBiLu)_3(FeAl)_5O_{12}$ layer that is characterized by a perpendicular anisotropy [16]. A strong direct exchange coupling is revealed via the formation of enlarged closure domains with a preferred orientation at the interface between the permalloy film and the garnet layer. As a result, the domain pattern of such a heterostructure shows an increased zero-field stripe period in comparison to the parent garnet layer [16]. The magnetization reversal process and magnetic domain structure were the focus points of these studies. YIG films with iron partially substituted with Co^{2+} and Co^{3+} ions [17] show interesting magnetic properties, such as several spin-reorientation phase transitions in a temperature range of 20–300 K [18], and both quasistatic [19] and ultrafast [20] light-induced changes in magnetic anisotropy. Light pulses excite large-angle magnetization precession in such garnets, the phase and the amplitude of the precession being determined by the polarization of the light. If coupled with a nanostructure ferromagnetic (metallic) overlayer, such photomagnetic effects in the garnet may also be transferred to the overlayer, thus creating new possibilities for ultrafast switching.

For instance, it is known for a metal/dielectric heterostructure that spin-orbital interaction may initiate a transfer of angular momentum between the layers and thus cause correlations in the magnetization dynamics [21]. Understanding optical control of the magnetism in magnetic heterostructures is a particularly important issue for further development of faster magnetic information storage/processing and spintronic nanodevices. Optical control of spins in Co/$SmFeO_3$ heterostructures by the X-ray pulse with duration 70 ps has been demonstrated using X-ray photoemission electron microscopy, revealing that the dynamics of the spins in the metallic Co and the dielectric $SmFeO_3$ are strongly coupled [22]. In the general case, a novel ultrafast magnetization dynamics in ferromagnetic metal/garnet heterostructures can be expected due to the coupling between the ferromagnetic and garnet films and/or the influence of the effective magnetic field of the ferromagnetic metallic film. Using the YIG:Co film in the

http://dx.doi.org/10.5772/62542

ferromagnetic/garnet heterostructures gives unique possibility to investigate light-induced magnetization dynamics at the sub-picosecond timescale.

This chapter describes experimental and theoretical studies of the magnetization behavior from statics to ultrafast light-induced magnetization dynamics in ultrathin 2 nm Co films deposited on Co-substituted yttrium iron garnet thin film. In particular, we demonstrate that ion beam sputtering can be used for the formation of Co/garnet heterostructures. The magnetization reversal process and magnetic anisotropy of the Co/garnet heterostructures are measured by both magneto-optical magnetometry and ferromagnetic resonance (FMR). To investigate the ultrafast magnetization dynamics in both garnet and Co/garnet heterostructure induced by femtosecond laser pulses, we carried out time-resolved measurements at room temperature using a magneto-optical pump-probe method. We demonstrated that the frequency of the spin precession in a Co/garnet bilayer can be modulated by exciting linearly polarized femtosecond pulses. The experimental results presented here were obtained on 2 nm Co/garnet heterostructure, which has a strong magnetostatic interlayer coupling. In this heterostructure, two distinct precession frequencies were observed. One is attributed to the magnetization precession of the 2 nm cobalt and the other to that of the 1.8-μm-thick garnet. The spin oscillation frequencies of the two layers differ by about a factor of two and are strongly dependent on the out-of-plane external magnetic field. We compared magnetization dynamics in the Co and bare garnet films separately via selective probing and showed that magnetization precession in the garnet via the photomagnetic effect can be manipulated by the magnetostatic interlayer coupling. The experimental results are discussed within the phenomenological model.

2. Heterostructure preparation

Initial garnet thin films composed of $Y_2Ca_1Fe_{3,9}Co_{0.1}Ge_1O_{12}$ (YIG:Co) were grown by liquid-phase epitaxy on $Gd_3Ga_5O_{12}$ (GGG) (001)-oriented substrate. The initial thickness of garnet films was 6.5 μm. The initial garnet surface was etching, and Co/YIG:Co heterostructures were formed using the dual ion beam sputtering technique [23] on the base of an A 700 Q Leybold vacuum system. The base pressure was below 8×10^{-6} mbar in the vacuum chamber. The damage-free etching of the garnet films and subsequent deposition of the Co layers were carried out *in situ* at a pressure of 2.5×10^{-4} mbar [24].

Figure 1 illustrates the stage of the heterostructure preparation. The initial garnet film was smoothed to 5.8 μm thickness with a 0.6-keV oxygen ion beam with current density of 0.2 mA/cm^2, corresponding to the ion flux of 3.2×10^{15} cm$^{-2} \times$ c^{-1} [24]. The oxygen ions improve garnet transmittance in the energy range between 0.5 and 1 keV. The garnet films are sputtered at a near-normal incidence angle. At this angle, optimal smoothing of the optical materials (quartz, glass, ceramic) is achieved for up to sub-nanometer roughness [25]. The garnet sputtering rate is about 0.22 μm/h. A final smoothing of the garnet surfaces was completed using a 0.3-keV oxygen ion beam for over 10 minutes. Au and Co targets were sputtered with a 1.5-keV argon ion beam at 0.25 mA/cm^2 current density [24]. The incident angle of argon ions is 60° with

respect to the target normal, so that the sputtered flux is deposited onto substrate at near-normal incidence angle. The deposition rates of Au and Co are 8.4 and 5.4 nm/min, respectively. A 4-nm Au film was used to protect the 2-nm Co layer before oxidation. For this thickness, the Au film is continuous and exhibits surface roughness close to the substrate of about 0.2 nm [26]. The Co/YIG:Co heterostructures and reference YIG:Co films are prepared onto the same substrate and in the same experimental conditions.

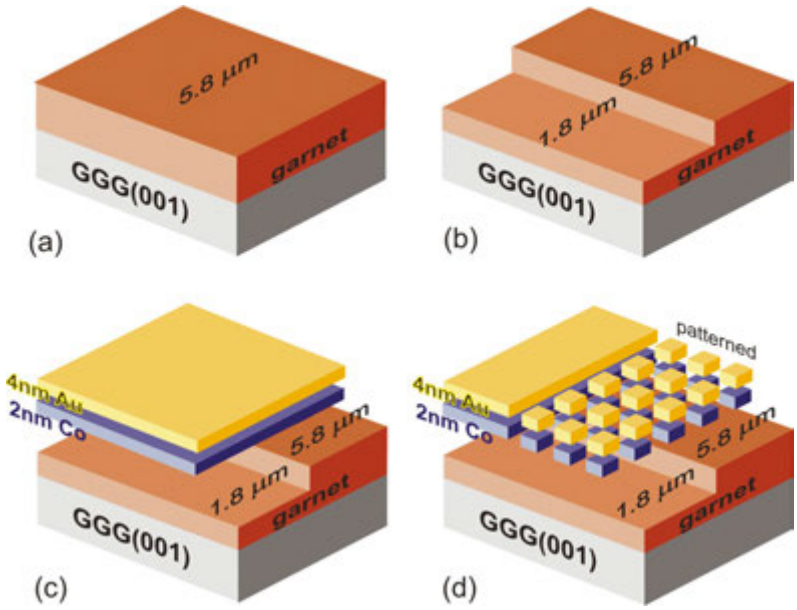

Figure 1. Schematic configuration of the heterostructure during preparation: (a) the YIG:Co film after smoothing from 6.5 μm to 5.8 μm thickness, (b) after ion beam etching to 1.8 μm on the garnet part, (c) after deposition of 4-nm Au/2 nm Co bilayer on the garnet part, and (d) the 20 × 20 μm pattern area on the Co/garnet part.

A 20 × 20 μm Au/Co pattern, for comparison of coupling between Co and garnet films and domain structures modifications on garnets, was fabricated by a lift-off photolithography. The photolithographic process can be represented as follows. In the first step, the garnet film was coated with the light-sensitive chemical photoresist to form a homogeneous layer of about 1 μm thickness. In the second step, the photoresist on garnet surface was exposed through a lithographic mask with high-intensity ultraviolet (UV) radiation. This mask contains the copy of pattern. The 20 × 20 μm windows are opened to the exposing UV light passes through the mask. The dose of UV exposure and the development process were precisely controlled to result in a sharp edge profile of resist patterns. In the third step, the irradiated photoresist area was washed away, leaving the photoresist in the unexposed area. In the fourth step, after deposition of the Au/Co bilayers, a chemical etching was used to remove the previously unexposed photoresist. In such way, the pattern from mask was transferred to the garnet film. As a result, the Co(homogeneous) and Co(pattern)/garnet heterostructures as well as reference

http://dx.doi.org/10.5772/62542

garnet films with discrete thicknesses were prepared onto the same GGG (001) substrate by combining the ion beam processing with photolithographic technique (see **Figure 1**).

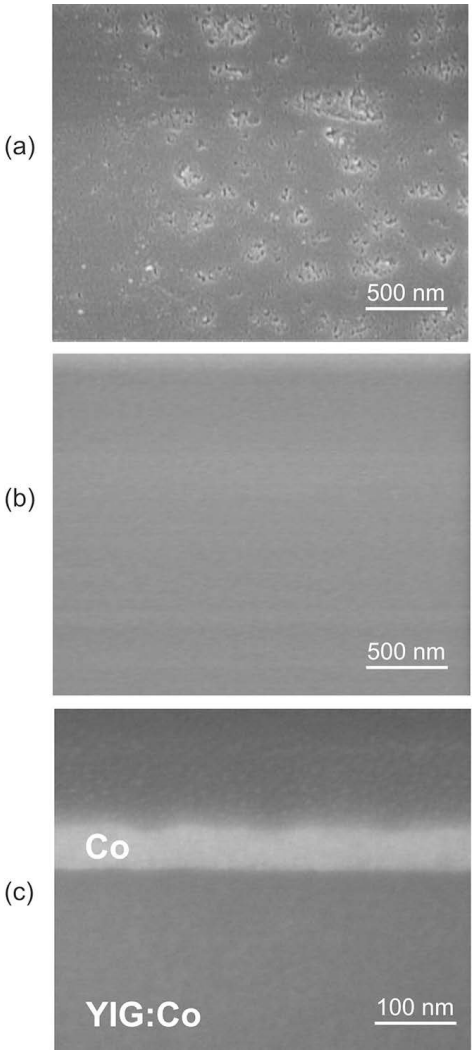

Figure 2. (a) SEM images of the initial 6.5 μm YIG:Co film, (b) 5.8 μm YIG:Co film after etching, of YIG:Co films, and (c) the cross-sectional image of the Co(50nm)/YIG:Co interface .

The surface morphology of both the bare YIG:Co film and Co/YIG:Co heterostructure was measured by high-resolution scanning electron microscopy (SEM) using a FEI's Helios NanoLab DualBeam system. The root mean square (rms) surface roughness was examined by atomic force microscope in tapping mode. The initial garnet surface is rough with protrusions,

while YIG:Co contains troughs of about 100–200 nm in diameter (see **Figure 2(a)**). The ion beam smoothing the garnet surface area showed significantly reduced rms parameters from 3.5 to 0.3 nm after etching the garnet film from 6.5 μm to 5.8 μm (see **Figure 2(b)**). The surface roughness remains approximately the same after ion beam etching down to 1 μm. Ion beam thinning of the garnet film also decreases the rms parameter to 0.25 nm. This is comparable to surfaces of roughness similar to high-quality Si substrate (0.18 nm).

The surfaces of the Co/garnet heterostructures are continuous and exhibit a slightly increased rms parameter from 0.3 to 0.37 nm after the deposition of Au(4nm)/Co(2 nm) bilayer structures on the ion beam-smoothed garnet surfaces. A cross section of the Co/garnet interface was observed using a 30-keV gallium-focused ion beam. The low contrast of the Co(≤5 nm)/garnet interfaces results from charge accumulation in the dielectric garnet film. Therefore, only for the SEM image observation, the thickness of the Co layer was increased up to 50 nm for the enhancement of the contrast at the Co/garnet interface. The Co/garnet interface is sharp, and the thickness of the transition layer is thinner than 1–2 nm (see inset of **Figure 2(c)**).

3. Optical and magnetic properties of Co/garnet heterostructures

The optical transmittance, magneto-optical both Kerr (θ_k) and Faraday (θ_F) rotations were performed on Co/YIG:Co heterostructures and reference YIG:Co film using light from a mode-locked Ti-sapphire laser (MaiTai HP, Spectra-Physics) operating within the 400–1040 nm range and a repetition rate of 80 MHz. For the detection of the angle of magneto-optical rotation, a lock-in amplifier was used in combination with a standard modulation technique with a photoelastic modulator.

3.1. Optical and magneto-optical spectra

The investigation of the optical absorption and the Faraday rotation spectra in YIG:Co garnet demonstrated that the contribution of Co ions in octahedral sites is substantially smaller than that of tetrahedral Co ions [27]. Furthermore, the latter can be observed in near-infrared range, where pure YIG is fully transparent. Both an optical transmittance and magneto-optical Faraday rotation spectra for YIG:Co film are shown in **Figure 3**. At wavelengths longer than about 800 nm, the absorption is small and is equal to about 10^2 cm^{-1} (see **Figure 3(b)**). Essentially in the wavelength range of 450–1300 nm, the absorption is caused by crystal field transitions of Fe^{3+}, Co^{2+}, and Co^{3+} ions in both tetrahedral and octahedral sites. The crystal field transitions in octahedral sites have weaker oscillator strength than that the tetrahedral ones. However, at wavelengths shorter than 450 nm, the strong optical absorption of the garnet film is related to charge transfer transitions from oxygen ligands O^{2-} to octahedral Fe^{3+} and Co^{3+} ions. The scheme of crystal field and charge transfer transitions for Co ions (**Figure 3(a)**) was obtained from experimental and theoretical investigations [27, 28]. In a band model, the charge transfer transition is connected with electron excitation from a valence band to conduction ones, which are created by O *2p* and Fe (Co) *3d* orbitals, respectively. Although a determination of band gap E_g is difficult owing to the garnets not exhibiting sharp absorption edge, the lowest charge transfer transitions of octahedral Co^{3+} ($^1A_1 \rightarrow {}^1T_2$) ions give $E_g \approx 2.85$ eV. This value agrees well

http://dx.doi.org/10.5772/62542

with the band gap of pure YIG (E_g = 2.9 eV). In the general case, the optical absorption is correlated with the magneto-optical Faraday rotation (defined by rotation angle θ_F) (see **Figure 3(c)**). The energy levels of the Co ions do not coincide with the *3d* levels of the Fe ions. Therefore, the optical excitation of YIG:Co film leads to additional transitions of Co ions as well as affect the Fe^{3+} ion transitions and consequently results in magneto-optical effects with spectral sensitivity.

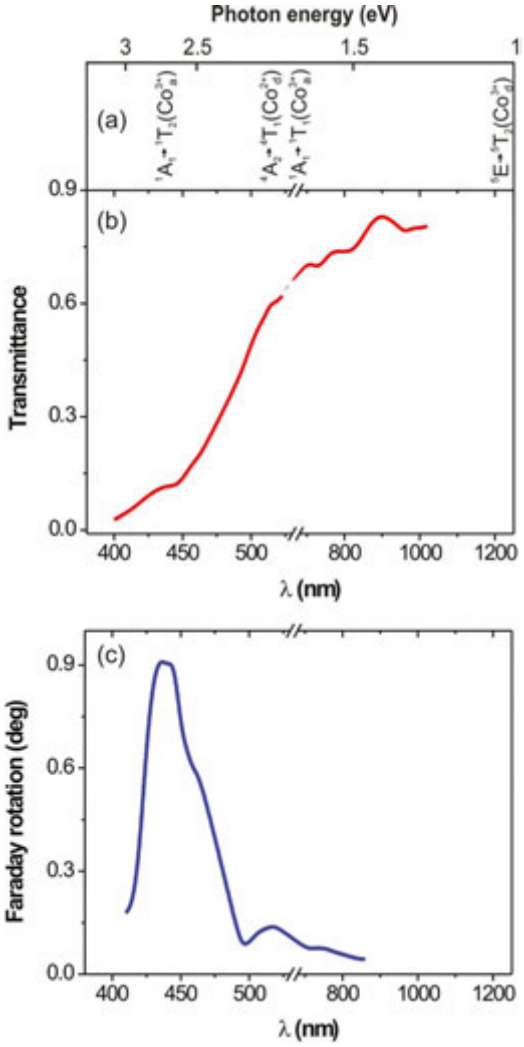

Figure 3. (a) Scheme of crystal field and charge transfer transitions according to Refs. [27, 28], (b) optical transmittance, and (c) magneto-optical Faraday rotation spectra of 1.8 μm YIG:Co film.

The contribution of Co ion transitions to magneto-optical Faraday rotation spectrum is clearly seen by comparison of previously reported spectra for both YIG [29] and YIG:Co films [27]. In our case, for the garnet film, we observed the reduction of θ_F close to the optical transitions of tetrahedral Co^{2+} and Co^{3+} ions as well as octahedral Co^{3+} ones. It is important to note that for different garnet thicknesses and both YIG and YIG:Co films reported, θ_F is practically the same in the wavelength range of 800–900 nm, where no optical transitions of Co ions are expected (see **Figure 3(b)**). This indicates that magnetic anisotropy (induced by the temperature, light, etc.) of the garnet can be modified due to inhomogeneous distribution of Co dopant in the garnet lattice. The contribution of low spin octahedral Co^{3+} ions to magnetic anisotropy is zero in single-ion approximation. Since tetrahedral Co^{2+} and Co^{3+} ions are responsible for growth-induced magnetic anisotropy [30], one can assume that the reduction in garnet thickness leads to a change in the uniaxial anisotropy and thus to a change in the magnetization reversal process. To confirm this, in the next sections we performed investigations of both the magnetic anisotropy and magnetization reversal processes in ultrathin Co layer and garnet thin films.

3.2. Magnetization reversal in static regime

The process of magnetization reversal has been studied at room temperature in reflection with the linear magneto-optic Kerr effect (MOKE) and in transmission with the Faraday effect. From the data, we separated different magneto-optical contributions from the Co layer and garnet-only films. The perpendicular magnetization component of the ultrathin Co layer was measured using the polar MOKE (P-MOKE) geometry, with the angle of incidence of the laser light close to the sample normal and the external magnetic field H_Z perpendicular to the surface of the sample (see **Figure 4(a)**). The measurements of the in-plane magnetization components of the Co layer were performed in the longitudinal MOKE (L-MOKE) geometry, with a 49° angle of incidence of the light (see **Figure 5(a)**). The magnetic field H_X was applied in the sample plane for various orientations with respect to the garnet [100] direction. The process of magnetization reversal to the determination of Faraday rotation angle θ_F of the garnet-only films was studied in the magneto-optical Faraday geometry, with perpendicular and in-plane magnetic field orientation (**Figure 4**).

According to the optical absorption spectra in **Figure 3(b)**, Au/Co/garnet heterostructures are transparent enough to be investigated in transmission geometry, for example at 690 nm wavelength. From the experimental curves, we separated the different magneto-optical contributions of the Co layer and garnet films using vector magneto-optical magnetometry and measurements for reference garnet film [31]. The P-MOKE hysteresis loops observed for the 2-nm-thick Co film grown on garnet film indicate an in-plane magnetization of Co (see **Figure 4(c)**). **Figure 4(b)** and **5(b)** show Faraday rotation hysteresis loops measured for garnet film and a perpendicular applied field H_Z and an in-plane field H_X, respectively. From the hysteresis loop shown in **Figure 4(b)**, one deduces a Faraday rotation from the garnet layer of about θ_F = 0.08 degrees and a paramagnetic linear contribution from the GGG substrate. For the in-plane applied magnetic field in the garnet [100] direction, the saturating field is about 0.6 kOe (**Figure 5(b)**).

http://dx.doi.org/10.5772/62542

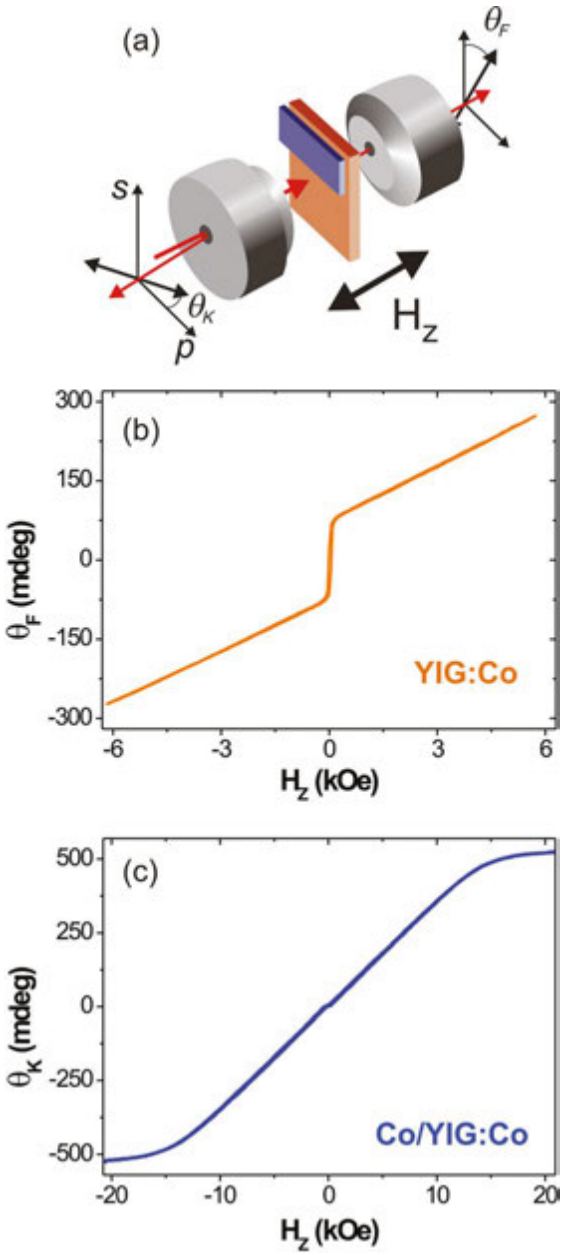

Figure 4. (a) The experimental configuration with Kerr and Faraday effects for perpendicular magnetic field orientation H_Z to the sample plane. Hysteresis loops measured for YIG:Co and Co/YIG:Co at 690 nm wavelength in: (b) Faraday and (c) P-MOKE geometries.

The L-MOKE magnetization curve for the Co layer measured with the in-plane external magnetic field H_X are shown in **Figure 5(c)**. From L-MOKE hysteresis loops, the remanence parameter is plotted on inset of **Figure 5(c)** as a function of azimuthal angle ϕ_H. The shape of these loops is practically independent on the azimuthal sample orientation and confirms the "easy plane" type of the magnetic anisotropy with a saturation in-plane field of about 0.3 kOe. To determine magnetic anisotropy of both garnet films and Co layer, we performed FMR measurements at room temperature.

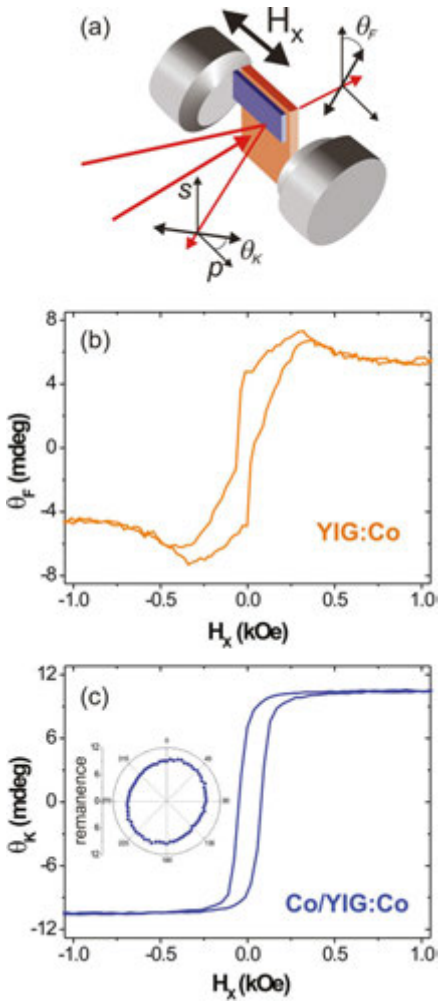

Figure 5. (a) The experimental configuration with Kerr and Faraday effects for sample in-plane magnetic field orientation H_X. Hysteresis loops measured for YIG:Co and Co/YIG:Co at 690 nm wavelength in: (b) Faraday and (c) L-MOKE geometries.

http://dx.doi.org/10.5772/62542

3.3. Magnetic anisotropy study

The typical FMR line measured in the external magnetic field applied to the sample at polar angle $\theta_H = 65°$ is presented in **Figure 6**. The Co layer and garnet film contributions to this FMR line can be clearly seen. The linewidth values of Co and garnet films are different. The peak-to-peak FMR linewidth ΔH is related to the relaxation rate of magnetization motion, which is caused by intrinsic Gilbert damping α and magnetic inhomogeneities $\Delta H(0)$ in ferromagnet: $H = \frac{2}{\sqrt{3}}\frac{\alpha}{\gamma}2\pi f_{FMR} + \Delta H(0)$, where γ is the gyromagnetic ratio, and f_{FMR} is the FMR frequency. The damping parameter estimated from above-mentioned ΔH values of Co and garnet films is equal to $\alpha_{Co} = 0.04$ and $\alpha_{garnet} = 0.19$. Nevertheless, the Gilbert damping of ultrathin Co layer grown on ultra-smoothed garnet film is comparable with the damping of high-quality single and polycrystalline Co layers obtained on metallic underlayers [32–34].

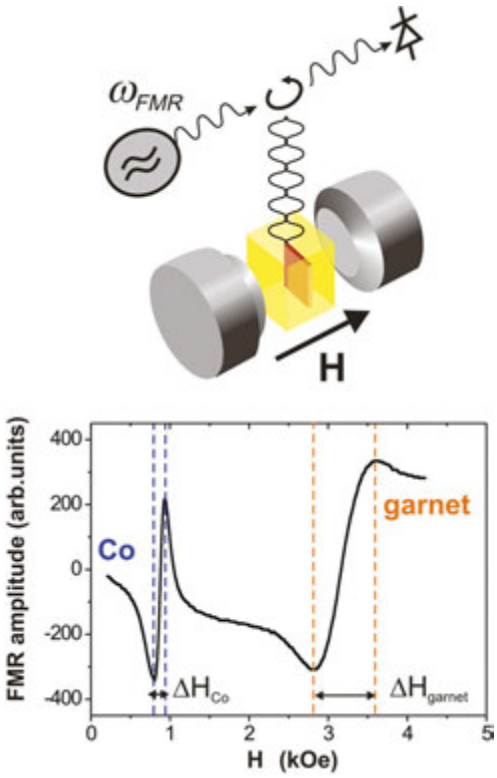

Figure 6. FMR lines for Co/YIG:Co heterostructure measured at $\theta_H = 65°$ and $\phi_H = 0°$ of the external magnetic field H.

The experimental dependencies of a resonance field H_R on the angles θ_H and ϕ_H for the garnet film and the Co layer are plotted in **Figures 7** and **8**, respectively. The existence of easy magnetization axes along the <111> directions for the garnet contributions was deduced by

analyzing $H_R(\theta_H,\phi_H)$ (see **Figure 7(a,b)**). This result correlates well with the Faraday experiments for garnet film, shown in **Figure 4(b)**. For the 2-nm Co layer, the easy magnetization axis lies in the sample plane (see **Figure 8(a)**) and is also connected with the "easy plane" type of the magnetic anisotropy (**Figure 8(b)**). As observed before, the magnetic anisotropy of the YIG:Co has two contributions [18]: magnetocrystalline cubic and growth-induced uniaxial ones. Hence, a qualitative analysis of the FMR and magnetization curves gives rise to the following description of the magnetic anisotropy energy E_A, which contains cubic, growth-induced and uniaxial anisotropies:

$$E_A\left(\vec{M}_{garnet},\vec{M}_{Co}\right)=K_1\left[\left(m_x m_y\right)^2+\left(m_x m_z\right)^2+\left(m_z m_y\right)^2\right]+K_{eff}^{garnet}\sin^2\theta+K_{eff}^{Co}\sin^2\theta_M \quad (1)$$

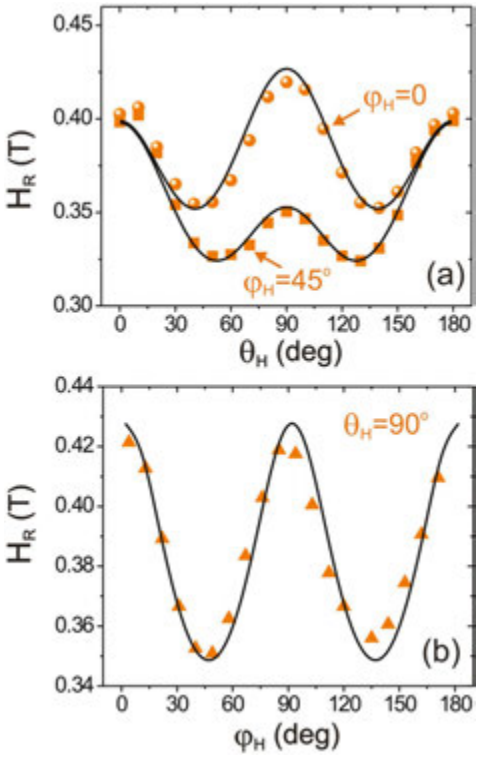

Figure 7. The polar (for $\phi_H = 0°$ and 45°) and azimuthal (for $\theta_H = 90°$) dependences of the resonance field H_R for YIG:Co film. The dots are experimental values, and solid lines were fitted using Eq. (1).

where $\vec{M}_{\text{garnet}}$ and $\vec{M}_{\text{Co}}$ are the magnetization vectors for garnet and Co films, respectively; K_C is the cubic anisotropy constant of garnet film; m_x, m_y, and m_z are the direction cosines of garnet magnetization vector along the principle crystallographic axes defined as $m_x = \sin\theta\cos\phi$, $m_y =$

http://dx.doi.org/10.5772/62542

$\sin\theta\sin\phi$, $m_z = \cos\theta$ (θ and ϕ are the polar and azimuthal angles of magnetization, respectively); $K_{\text{eff}}^{\text{garnet}}$ is the effective growth-induced (uniaxial) anisotropy constant for the garnet film, $K_{\text{eff}}^{\text{Co}}$ is the effective uniaxial anisotropy constant of the 2-nm Co layer defined by the polar angle θ_M. The bulk value of the saturation magnetization 1420 G was assumed for the 2-nm Co thickness. The saturation magnetization was 7 G [17]. For each resonance line of YIG:Co and ultrathin Co films, the magnetic anisotropy constants were fitted using Eq. (1) and standard FMR conditions [35, 36]:

$$f_{FMR} = \frac{1}{2\pi}\frac{\gamma}{M\sin\theta}\left[\frac{\partial^2 E_A}{\partial\theta^2}\frac{\partial^2 E_A}{\partial\varphi^2} - \left(\frac{\partial^2 E_A}{\partial\theta\partial\varphi}\right)^2\right]^{1/2} \tag{2}$$

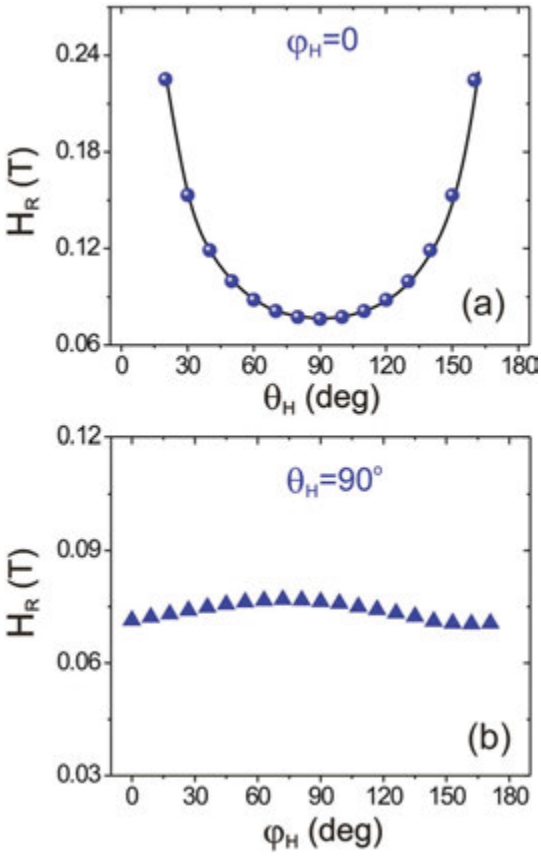

Figure 8. The polar (for $\phi_H = 0°$ and 45°) and azimuthal (for $\theta_H = 90°$) dependences of the resonance field H_R for 2-nm Co layer on YIG:Co film. The dots are experimental values, and the solid line was fitted using Eq. (1).

where f_{FMR} is the FMR frequency. The equilibrium angles θ and ϕ of the magnetization can be found by the minimization of E_A: $\frac{\partial E_A}{\partial \theta}=0$ and $\frac{\partial E_A}{\partial \phi}=0$. The FMR frequency was $f_{FMR}=9.5$ GHz (X-band spectrometer). The gyromagnetic ratio of Co layer and garnet films is suggested to be equal to $\gamma_{Co}=1.76\times10^6$ Hz/Oe and $\gamma_{garnet}=1.65\times10^6$ Hz/Oe, respectively. The gyromagnetic ratio values of Co and garnet films correspond to the factors $g_{Co}=2$ and $g_{garnet}\approx1.9$, which are comparable to the previously reported experimental data for Co [35] and the similar garnet compositions [37, 38]. The reduction of g_{garnet} can be explained in terms of Wangsness model for the two-sublattice ferrimagnet [39]. The first sublattice is produced by tetrahedral and octahedral Fe^{3+} ions for which the g-factor is close to two, while second one is formed by high-spin octahedral Co^{2+} ions with $g\approx2.9$ [38]. As a result, oppositely directed sublattices lead to the reduction of the effective g-factor. Solid lines in **Figures 7** and **8** show the results of the fitting procedure.

Thus, let us analyze, step by step, the magnetic anisotropy constants of the Co layer and garnet films from FMR field and magnetization loops. First, for the Co layer deposited on the garnet film, the effective anisotropy constant is $K_{eff}^{Co}=-9.9\times10^6 erg/cm^3$ that corresponds to the case of in-plane magnetic anisotropy in the Co layer. Second, from the part of FMR spectrum which corresponds to garnet films, the cubic $K_C=-2\times10^3$ erg/cm^3 anisotropy contribution for garnet film was deduced from the fitting procedure. In the case of negative K_C, four easy magnetization-axis orientations along a <111>-type of crystallographic direction to the sample plane in garnet films exist [39]. Third, cubic constants K_C determined by FMR technique were used for the fitting of Faraday loops measured for garnet parts of a sample. Since the direction of magnetization at equilibrium corresponds to the minimum of $E_A(M_{garnet})$, the effective growth-induced anisotropy constant $K_{eff}^{garnet}=K_U^{garnet}-2\pi M_{garnet}^2$ can be determined from the minimization of $E_A(M_{garnet})$ with respect to the polar angle θ of magnetization: $\frac{\partial E_A(M_{garnet})}{\partial \theta}=0$. After separation of the demagnetization contribution from the uniaxial anisotropy, the anisotropy constant $K_U^{garnet}=10^3 erg/cm^3$ for 1.8-μm-thick garnet film was obtained [40].

3.4. Magnetostatic interlayer coupling

Here, we report on an influence of the 2-nm Co layer on both the domain structure geometry and magnetization reversal processes in the YIG:Co film. The period and shape of domains in Co/YIG:Co heterostructure are explained by competition of different energies. Taking into account the domain period in garnet film of order of 10 μm, the 20 × 20 μm Au/Co pattern is required for the observation of domain structure of garnet films under ultrathin Co layer [40], i.e., the size of pattern square is larger than domain period of garnet films. **Figure 9** shows the images of domain structure for patterned Co/garnet area recorded at $H_Z=0$ and $H_Z=40$ Oe, respectively.

http://dx.doi.org/10.5772/62542

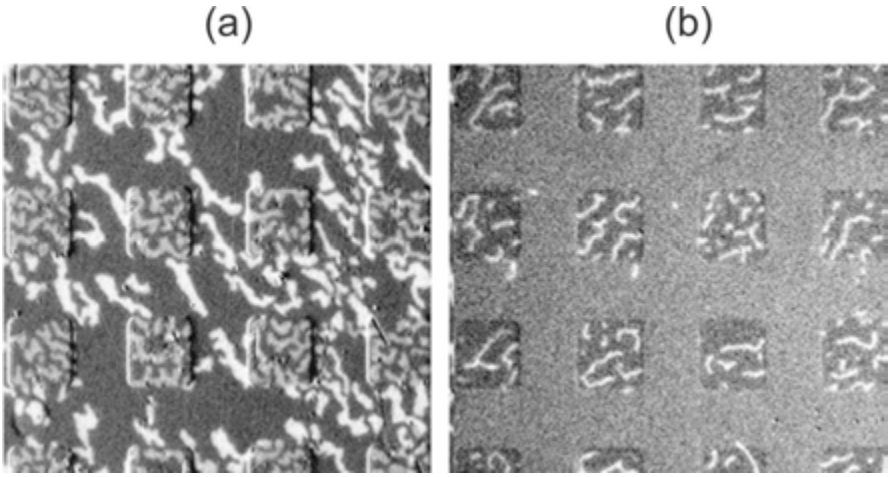

Figure 9. Images of magnetic domain structure in 2-nm Co/YIG:Co pattern area recorded at: (a) $H_Z = 0$ and (b) $H_Z = 40$ Oe. The image size is 140 × 130 μm.

In **Figure 9(a)**, both in garnet and Co/garnet (square areas) structures, stripe domain structures are observed. In this case, the period and the domain size in the Co/garnet structure is less than in the garnet film.

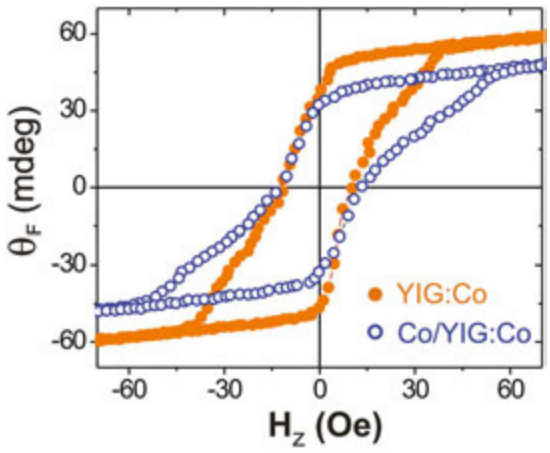

Figure 10. The hysteresis loops recorded for both bare YIG:Co (full points) and Co/YIG:Co (open points) films.

At $H_Z = 40$ Oe, the domain structure was observed only at Co/garnet pattern (see **Figure 9(b)**). Moreover, the clear difference in the magnetization reversal process with and without the 2-

nm cover Co layer on garnet film was observed in the field range near the coercivity (see **Figure 10**). First, for Co/garnet heterostructure, we observe the reduced θ_F value compared to the bare garnet film, i.e., the contribution of the hard axis from the Co/garnet interface to hysteresis loop is found. Second, the value of the reversal magnetic collapse field is noticeably increasing from 40 to 55 Oe. In **Figure 9(b)**, the presence of Co/garnet domains on a monodomain background garnet area is well visible. In this case, the extra energy is required to switch the in-plane interfacial magnetic moment in the garnet film. For these reasons, the strong in-plane magnetic anisotropy of the ultrathin Co layer induces significant stray field on the garnet surface. Therefore, for the Co/garnet heterostructure, reduction of the domain period occurs as a consequence of decreasing the magnetostatic energy.

4. Ultrafast magnetization dynamics induced by femtosecond laser pulses in a Co/garnet heterostructure

We present the results of a study of ultrafast photoinduced magnetization dynamics in Co/YIG:Co heterostructures via the excitation of photomagnetic anisotropy [19, 20]. This anisotropy is related to an optically induced charge transfer between the anisotropic Co^{2+} and Co^{3+} ions on tetrahedral sites in the garnet lattice. The deposition of ultrathin Co layer on garnet film can result in a new type of magnetization dynamics due to the influence of the effective magnetic field of the Co layer and/or the magnetic coupling between the metallic layer and garnet film.

4.1. Time-resolved magneto-optical tools

To investigate the ultrafast magnetization dynamics in both bare YIG:Co film and Co/YIG:Co heterostructure induced by femtosecond laser pulses, we carried out time-resolved measurements at room temperature using a conventional magneto-optical pump-probe method. Pump pulses with a duration of 35 fs from an amplifier (Spitfire Ace, Spectra-Physics) at a 500 Hz repetition rate were directed at an angle of incidence about 10° from the sample normal parallel to the [001] crystallographic axis of the sample, while the probe pulses at a 1 kHz repetition rate of the pump were incident along the sample normal, see **Figure 11**. A pump beam with a wavelength of 800 nm and energy of 2 μJ was focused onto a spot about 100 μm in diameter on the sample. The pump energy was relatively small in order to not heat significantly the metallic layers of Au and Co. The sample was excited by the pump through the Co side of the bilayer. A probe beam with a wavelength of 800 nm was about two times smaller in size and the energy than the pump. The parameter of delay time Δt (see **Figure 1**) between the pump and the probe pulses could be adjusted up to 1.3 ns. The linear polarization of the pump beam was defined by angle φ to the [100] axis. The amplitude of the magnetization precession was maximal when the polarization plane of the pump was along [100] or [010] axes. On the contrary, the polarization of the probe beam was along the [1–10] axis.

http://dx.doi.org/10.5772/62542

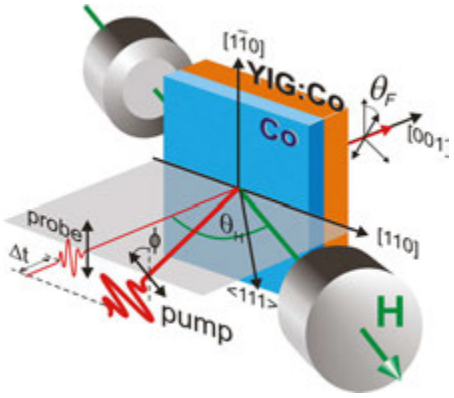

Figure 11. Sample configuration and the experimental geometry with the external magnetic field H applied with angle $\theta_H = 65^\circ$.

In this experimental geometry, we measured the Faraday rotation angle θ_F of the probe as a function of the delay time Δt between the pump and probe pulses. The rotation $\theta_F(\Delta t)$ is proportional to the out-of-plane component of the magnetization M_Z. An external magnetic field H up to 5 kOe was applied along the (1–10)plane at $\theta_H = 65°$ with respect to the sample normal. At the same time, H was above domain collapse field, so that a coherent spin dynamics without domain structure was investigated.

4.2. Spin precession modulation

The experimental results presented below were obtained on 2-nm Co/YIG:Co heterostructure, in which strong magnetostatic interlayer coupling has been found. **Figure 12** shows the magnetization precession (angle of Faraday rotation) as a function of the delay time Δt for different values of the amplitude of the external magnetic field with angle $\theta_H = 65^\circ$. We expect that the magnetization dynamics corresponds to a precession of the Co and garnet moments around the effective field. For a relatively small external magnetic field, one can find a slow oscillation with a main single frequency of 4.2 GHz, see **Figure 12(a)**, corresponding to the garnet film [41]. We observe periodic oscillation modulated by a higher-frequency oscillation in **Figure 12(b)**. Fast Fourier transforms (FFTs) were taken for these dependences, and the resulting power spectra confirm the presence of two different oscillation frequencies f_1 and f_2 (see **Figure 12(b)**). Both of these frequencies increase with increasing amplitude of the external magnetic field. However, we observed a main single higher oscillation frequency for the external magnetic field above 4 kOe (see **Figure 12(c)**). The Faraday rotation transients for varying external magnetic field H were fitted (**Figure 12**) with two damped sine contributions:

$$\theta_F(\Delta t) = A_1 \exp\left(\frac{-\Delta t}{\tau_1}\right)\sin\left(2\pi f_1 \Delta t + \phi_1\right) + A_2 \exp\left(\frac{-\Delta t}{\tau_2}\right)\sin\left(2\pi f_2 \Delta t + \phi_2\right) \quad (3)$$

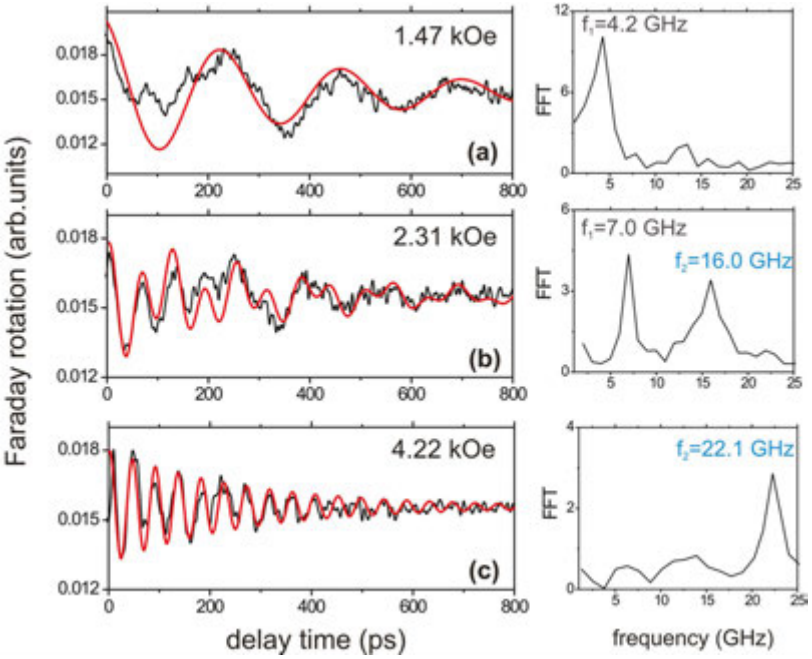

Figure 12. Time-resolved Faraday rotation as a function of the delay time Δt for (a) H = 1.47 kOe, (b) 2.31 kOe, and (c) 4.22 kOe. The red solid lines were fitted using FFT analysis and Eq. (3). The right panel—the FFT spectra.

where τ_i is the time decay, A_i the amplitude, and φ_i the phase. The fitted curves using FFT analysis and Eq. (3) are in good agreement with the experimental data (see **Figure 12**).

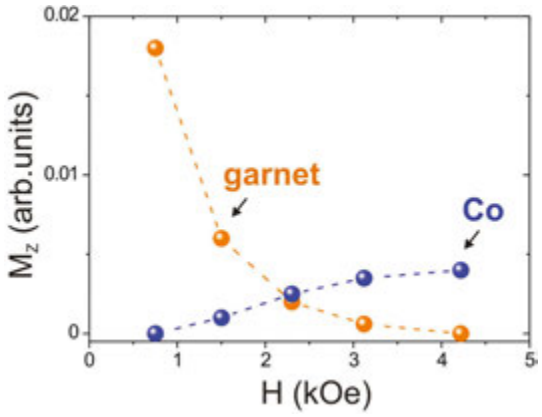

Figure 13. Dependence of the magnetization component M_Z on the amplitude of external field H for the garnet and Co layer.

http://dx.doi.org/10.5772/62542

From the experimental curves, we deduced amplitudes of the oscillations using fitting by Eq. (3). It is clearly seen that upon increasing H, the contribution from the garnet vanishes so that at the field above 4 kOe, the contribution from the Co layer dominates (see **Figure 13**). The dependence of perpendicular component of the magnetization M_Z is proportional to the Faraday rotation θ_F.

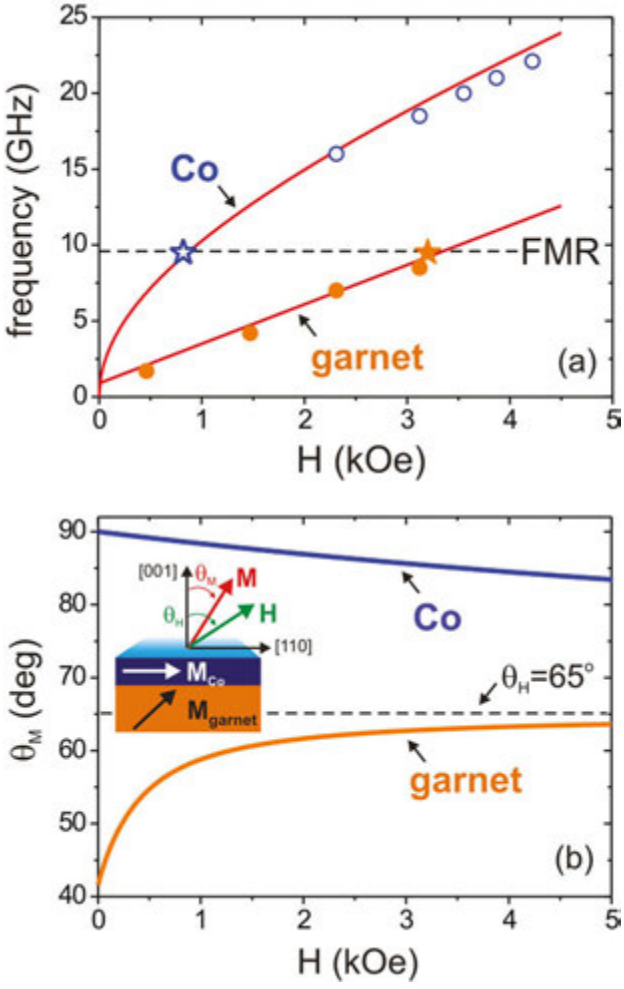

Figure 14. (a) Dependence of the frequency of magnetization precession on a function of magnetic field amplitude H for garnet (full points) and Co (open points) films of a heterostructure. The calculated FMR frequency dependences are shown using both Eqs. (1) and (2) with magnetic anisotropy constants (solid lines). The measured FMR data are shown as stars. (b) Calculation of magnetization orientation θ_M as a function of the amplitude of H for YIG:Co film and 2-nm Co layer.

Figure 14(a) plots the frequencies f_1 and f_2 obtained from experimental data for different values of the H. The dashed line is determined by the FMR frequency where the resonance field values for Co and garnet films are located (stars). To compare obtained frequencies, we calculated the FMR frequency as a function of the external magnetic field with angle $\theta_H = 65^\circ$ in both the cobalt and garnet films using a typical FMR equation [35], considering constants of the magnetic anisotropy of the 2-nm Co and 1.8 μm garnet film. The frequencies f_1 and f_2 differing by about a factor of two correspond to the precession of the magnetization excited in garnet and Co films, respectively. We see from **Figure 14(a)** that the experimental magneto-optical response data (points) agree well with the measured FMR results with single 9.5 GHz frequency (stars) and calculated FMR frequency (solid lines) for both contributions in the bilayer using Eq. (2).

Such a layer selective probing of the magnetization dynamics can be understood by a simple phenomenological model. The equilibrium state of magnetization vector at the Co/YIG:Co heterostructure could be found using the phenomenological model of magnetic anisotropy (Eq. (1)) after minimizing the total energy including energies of the magnetic anisotropies, the Zeeman at external magnetic field, and the demagnetization. **Figure 14(b)** shows the dependence of magnetization angle θ_M, on an external magnetic field H for both Co and garnet films. According the Faraday configuration, the polarization rotation of the probe beam was proportional to the perpendicular magnetization component along [001] axis at the garnet (see **Figure 11**). Thus, θ_F is proportional to the amplitude of the magnetization precession. During increasing θ_M, we observed increasing the amplitude of the magnetization precession. A quantitative analysis of dependences of the angle on the external magnetic field shows the possibility of the excitation of magnetization precession at two regimes: first, at low magnetic field below 1 kOe, the amplitude of magnetization precession dominates at the garnet film due to the large angle between magnetic field H and magnetization of garnet M_{garnet} and small perpendicular magnetization component of cobalt M_{Co}; second, at high magnetic field above 4 kOe, the amplitude of magnetization precession is dominated at the Co film with the significant perpendicular component M_{Co} when the magnetization vector M_{garnet} is close to H.

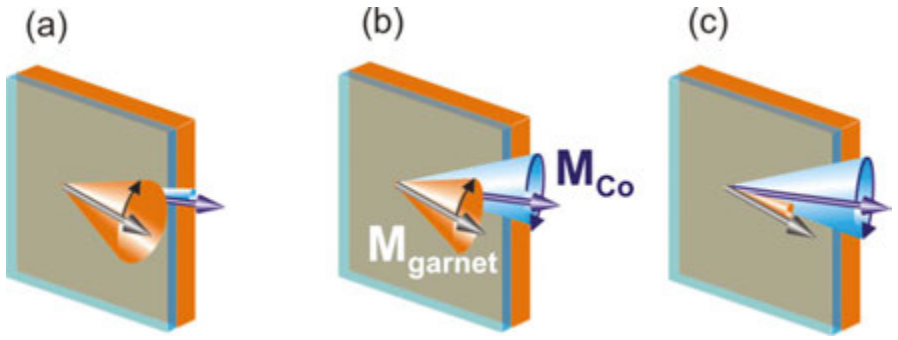

Figure 15. Graphical illustration of the precessional dynamics for: (a) $H < 1.5$ kOe, (b) $1.5 < H < 4.3$ kOe, and (c) $H > 4.3$ kOe.

http://dx.doi.org/10.5772/62542

We can conclude that we observe three types of magnetization precession in the bilayer: (i) mainly single-frequency precession (1–5 GHz) from the garnet for $H < 1.5$ kOe, (ii) a double frequency to modulated signal for $1.5 < H < 4.3$ kOe, and (iii) mainly single-frequency precession (>20 GHz) from the cobalt film for $H > 4.3$ kOe (see the graphical illustration of the precessional dynamics in **Figure 15**).

4.3. Laser-induced phase-sensitive magnetization precession

In this part, we compare magnetization dynamics in the Co and bare garnet films separately via selective probing and show that magnetization precession in the garnet can be manipulated by magnetostatic interlayer coupling.

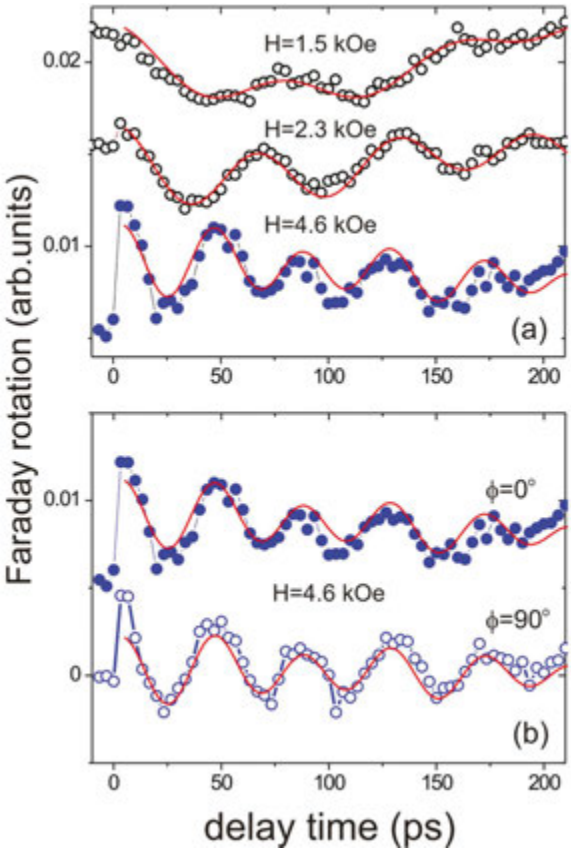

Figure 16. Time-resolved Faraday rotation of the Co/garnet heterostructure as a function of the delay time Δt for different (a) magnetic field amplitude and (b) pump polarization. Solid line was fitted using the classical oscillation function including damping for a 2-nm Co layer on a garnet film.

A rather unique combination of magnetic properties of the layers allows us to realize different regimes of the laser-induced dynamics. Changing the strength of the out-of-plane H, we were able to obtain conditions when the magnetization dynamics was dominated either by the Co or the garnet layer. As discussed in the previous part, for $H < 1$ kOe photoinduced dynamics of Co/garnet, the heterostructure is dominated by the magnetization precession of the garnet film, while at $H > 4$ kOe, the magnetization precession results from the Co layer. Time dependence of the z-component of the magnetization precession was on the function of the external magnetic field H and the angle of polarization plane of the pump beam. **Figure 16(a)** shows the magnetization precession curves measured at $H = 1.5$ kOe, 2.3 kOe, and 4.6 kOe for $\varphi = 0^{o}$. The laser-excited precessions of the magnetizations at two different frequencies are deduced from **Figure 14** as FMR frequencies in both the Co and the garnet films.

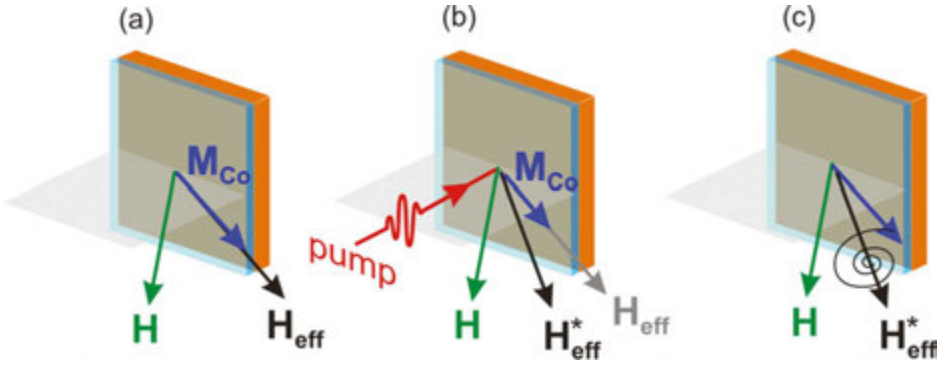

Figure 17. Graphical illustration of an ultrafast demagnetization dynamics in a 2-nm Co layer for (a) $\Delta t < 0$, (b) $0 < \Delta t < t_w$ (pulse duration), and (c) $\Delta t > t_w$.

The photoinduced magnetization precession for different pump beam polarizations at an external magnetic field with 4.6 kOe is shown in **Figure 16(b)**. These curves demonstrate no polarization dependence of the magnetization precession [42]. For such metallic ferromagnets, the ultrafast light-induced demagnetization is typical [43, 44]. The thermal demagnetization is seen as a sub-picosecond change of the magneto-optical signal measured at $H = 4.6$ kOe. The observed light-induced magnetization dynamics is a result of temperature increase of electron system on femtosecond timescale and a subsequent ultrafast reduction of M_{Co} [45], which effectively change the equilibrium orientation of the magnetization in this layer and thus triggers spin oscillations (see the graphical illustration in **Figure 17**).

To study the influence of the Co film on the ultrafast magnetization dynamics at the garnet film, the time-resolved Faraday measurements at low-field regime below 1 kOe were performed [42]. In this case, the amplitude of magnetization precession at YIG:Co film always dominates that of the Co film (see **Figure 13**). First, we measured the laser-induced magnetization dynamics in a bare garnet film. **Figure 18(a)** shows that changing the polarization of the pump induces a shift of the phase of the precession $\Delta\psi = 120^{o}$ in the bare garnet film. In this case, the decay coefficient of photoinduced anisotropy is $\tau_g \sim 20$ ps. In case of the deposition

http://dx.doi.org/10.5772/62542

of the 2-nm Co film on this garnet film, the polarization sensitivity of the magnetization precession disappears. The polarization angles of pump beam with φ = 0 and 90° trigger magnetization precession in YIG:Co with the same phase ($\Delta\psi \approx 0$), see **Figure 18(b)**. The time of relaxation of magnetization precession after pump pulse is $\tau_c \sim 60$ ps. This value is enlarged due to the influence of light-induced demagnetization at Co layer. The magnetization dynamics triggered in YIG:Co film and the Co/YIG:Co heterostructure with the same polarization of the pump light are clearly different. However, the frequencies of these precessions are similar.

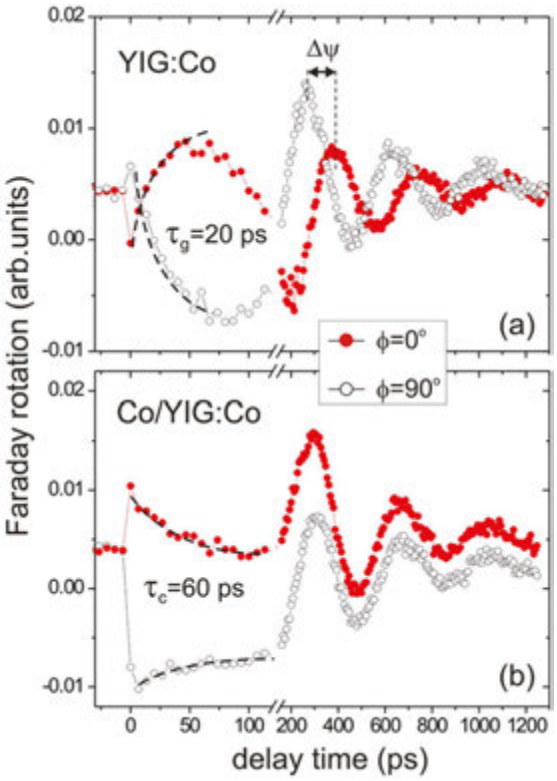

Figure 18. Time-resolved Faraday rotation of (a) bare garnet and (b) Co/garnet films as a function of the delay time Δt for $H(\theta_H = 65°) = 0.75$ kOe and different pump polarization φ. Dashed lines were fitted using the exponential function with decay coefficients τ_L.

The laser excitation of Co/YIG:Co heterostructure leads to both an thermal demagnetization at Co film and a photomagnetic effect at the garnet [20]. These effects induced changing the magnetization orientation given by the effective field H_{eff} in the heterostructure (see **Figure 17**). In this case, ultrafast change triggers the precession of the magnetization vector around the new orientation H^*_{eff} (see **Figure 17(c)**). In YIG:Co, the polarization-dependent excitation with different initial phase of magnetization precession leads to a photoinduced magnetic

anisotropy [19]. However, in our heterostructure, the phase of magnetization precession is defined by both the effective anisotropy (magnetocrystalline, uniaxial, and photoinduced) field and the stray field from 2-nm Co film (the magnetization of cobalt is significant larger than the magnetization of garnet). The magnetostatic coupling between Co and YIG:Co films leads to a change in the phase of magnetization precession in YIG:Co film. Thus in heterostructure, the magnetization is precessed around the effective magnetic field with the isotropic in-plane component due to the ”easy plane” of magnetic anisotropy of Co film.

5. Conclusion

In this chapter, we have presented the experimental investigation of ultrathin Co/garnet heterostructure by using time-resolved pump-probe magneto-optical spectroscopy in combination with linear magneto-optical Faraday and Kerr effects and ferromagnetic resonance. Ion beam processing procedure for preparation of Au/Co/garnet heterostructure with a subnanometer roughness parameter at the interface has been proposed. It was found that Gilbert damping of the ultrathin Co layers on the garnet surfaces is comparable to the damping of high-quality single and polycrystalline Co layers grown on metallic underlayers. We showed that the magnetic and magneto-optical properties of Co/garnet heterostructures can be engineered by covering the ultrathin Co layer. In particular, a strong magnetostatic interlayer coupling between the 2-nm Co layer and YIG:Co film has been found. In addition, the modification of the domain structure due to the magnetostatic coupling has been demonstrated. In principle, depositing ultrathin ferromagnetic layers on a garnet film can also lead to new effects in magnetization dynamics, due to the influence of the effective magnetic field of the ferromagnetic layer and/or the coupling between ferromagnetic layer and garnet.

The growth of a 2-nm Co layer on top of the garnet significantly changes the mechanism of the laser-induced precession in the heterostructure. We observed the modulation of spin precession in a Co/garnet heterostructure with distinct frequencies. The excitation efficiency of these precessions strongly depends on the amplitude and orientation of external magnetic field. In addition, we demonstrate that the laser pulse triggers polarization-independent precession in both the Co and garnet layers via the magnetostatic coupling between these layers.

These results demonstrate that magnetic metal/dielectric heterostructures are interesting and promising objects for further investigations of all-optical ultrafast light-induced phenomena and their potential applications.

Acknowledgements

This work was supported by the National Science Centre Poland for OPUS project DEC-2013/09/B/ST3/02669. The author would like to acknowledge the contributions of M. Pashkevich for measurements and A. Stognij for heterostructures preparation. The author is

grateful to M. Tekielak, R. Gieniusz, A. Maziewski, A. Kirilyuk, A. Kimel, and T. Rasing for fruitful discussions and research support.

Author details

Andrzej Stupakiewicz

Address all correspondence to: and@uwb.edu.pl

Laboratory of Magnetism, Faculty of Physics, University of Bialystok, Bialystok, Poland

References

[1] A. Kirilyuk, A. V. Kimel and Th. Rasing. Ultrafast optical manipulation of magnetic order. Rev. Mod. Phys.. 2010;82:2731.

[2] E. Beaurepaire, J.-C. Merle, A. Daunois, and J.-Y. Bigot. Ultrafast Spin Dynamics in Ferromagnetic Nickel. Phys. Rev. Lett.. 1996;76:4250.

[3] U. Bovensiepen. Femtomagnetism: Magnetism in step with light. Nature Physics. 2009;5:461.

[4] I. Radu, K. Vahaplar, C. Stamm, T. Kachel, N. Pontius, H. Dürr, T. Ostler, J. Barker, R. Evans, R. Chantrell, A. Tsukamoto, A. Itoh, A. Kirilyuk, Th. Rasing, A. Kimel. Transient ferromagnetic-like state mediating ultrafast reversal of antiferromagnetically coupled spins. Nature. 2011;472:205.

[5] B. Koopmans, G. Malinowski, F. Dalla Longa, D. Steiauf, M. Fähnle, T. Roth, M. Cinchetti and M. Aeschlimann. Explaining the paradoxical diversity of ultrafast laser-induced demagnetization. Nature Mat.. 2010;9:259.

[6] W. A. Challener, C. Peng, A. V. Itagi, D. Karns, W. Peng, Y. Peng, X.-M. Yang, X. Zhu, N. J. Gokemeijer, Y.-T. Hsia, G. Ju, R. E. Rottmayer, M. A. Seigler and E. C. Gage. Heat-assisted magnetic recording by a near-field transducer with efficient optical energy transfer. Nature Photon.. 2009;3:220.

[7] V.I. Belotelov, I.A. Akimov, M. Pohl, V.A. Kotov, S. Kasture, A.S. Vengurlekar, Achanta Venu Gopal, D.R. Yakovlev, A.K. Zvezdin, M. Bayer. Enhanced magneto-optical effects in magnetoplasmonic crystals. Nature Nanotech.. 2011;1:370.

[8] T. Satoh, Y. Terui, R. Moriya, B. A. Ivanov, K. Ando, E. Saitoh, T. Shimura, and K. Kuroda. Directional control of spin-wave emission by spatially shaped light. Nature Photon.. 2012;6:662.

[9] S. Parchenko, A. Stupakiewicz, I. Yoshimine, T. Satoh, and A. Maziewski. Wide frequencies range of spin excitations in a rare-earth Bi-doped iron garnet with a giant Faraday rotation. Appl. Phys. Lett.. 2013;103:172402.

[10] S.O. Demokritov, V.E. Demidov, O. Dzyapko, G.A. Melkov, A.A. Serga, B. Hillebrands, A.N. Slavin. Bose–Einstein condensation of quasi-equilibrium magnons at room temperature under pumping. Nature. 2006;443:430.

[11] A.B. Chizhik, I.I. Davidenko, A. Maziewski, A. Stupakiewicz. High-temperature photomagnetism in Co-doped yttrium iron garnet films. Phys. Rev. B. 1998;57:14366.

[12] F. Hansteen, A. V. Kimel, A. Kirilyuk, and Th. Rasing. Femtosecond Photomagnetic Switching of Spins in Ferrimagnetic Garnet Films. Phys. Rev. Lett.. 2005;95:047402.

[13] A. V. Kimel, A. Kirilyuk, P. A. Usachev, R. V. Pisarev, A. M. Balbashov and Th. Rasing. Ultrafast non-thermal control of magnetization by instantaneous photomagnetic pulses. Nature. 2005;435:655.

[14] S. Parchenko, T. Satoh, I. Yoshimine, F. Stobiecki, A. Maziewski, and A. Stupakiewicz. Non-thermal optical excitation of terahertz-spin precession in a magneto-optical insulator. Appl. Phys. Lett.. 2016;108:032404.

[15] Y. S. Chun and Kannan M. Krishnan. Interlayer perpendicular domain coupling between thin Fe films and garnet single-crystal underlayers. J. Appl. Phys.. 2004;95:6858.

[16] N. Vukadinovic, J. Ben Youssef, V. Castel, M. Labrune. Magnetization dynamics in interlayer exchange-coupled in-plane/out-of-plane anisotropy bilayers. Phys. Rev. B. 2009;79:184405.

[17] A. Maziewski. Unexpected magnetization processes in YIG+Co films. J. Magn. Magn. Mater.. 1990;88:325.

[18] M. Tekielak, A. Stupakiewicz, A. Maziewski and J. M. Desvignes. Temperature induced phase transitions in Co-doped YIG films. J. Magn. Magn. Mater. 2003;254–255:562.

[19] A. Stupakiewicz, A. Maziewski, I. Davidenko, and V. Zablotskii. Light-induced magnetic anisotropy in Co-doped garnet films. Phys. Rev. B.. 2001;64:064405.

[20] F. Atoneche, A.M. Kalashnikova, A.V. Kimel, A. Stupakiewicz, A. Maziewski, A. Kirilyuk, and Th. Rasing. Large ultrafast photoinduced magnetic anisotropy in a cobalt-substituted yttrium iron garnet. Phys. Rev. B. 2010;81:214440.

[21] G. Woltersdorf, O. Mosendz, B. Heinrich and C.H. Back. Magnetization Dynamics due to Pure Spin Currents in Magnetic Double Layers. Phys. Rev. Lett.. 2007;99:246603.

[22] L. Le Guyader, A. Kleibert, F. Nolting, L. Joly, P. M. Derlet, R. V. Pisarev, A. Kirilyuk, Th. Rasing and A. V. Kimel. Dynamics of laser-induced spin reorientation in Co/SmFeO3 heterostructure. Phys. Rev. B. 2013;87:054437.

[23] I. G. Brown. The Physics and Technology of Ion Sources. NewYork: Wiley; 2004.

[24] M. Pashkevich, R. Gieniusz, A. Stognij, N. Novitskii, A. Maziewski, and A. Stupakiewicz. Formation of cobalt/garnet heterostructures and their magnetic properties. Thin Solid Films. 2014;556:464.

[25] A. Keller, S. Facsko and W. Möller. The morphology of amorphous SiO2 surfaces during low energy ion sputtering. J. Phys.: Condens. Matter.. 2009;21:495305.

[26] A. I. Stognij, N. N. Novitskii, S. D. Tushina, S. V. Kalinnikov. Preparation of ultrathin gold films by oxygen-ion sputtering and their optical properties. Technical Physics. 2003;48:745.

[27] Z. Šimša. Optical and magnetooptical properties of Co-doped YIG films. Czech. J. Phys. B. 1984;34:78.

[28] D.L. Wood and J.P. Remeika. Effect of Impurities on the Optical Properties of Yttrium Iron Garnet. J. Appl. Phys.. 1967;38:1038.

[29] Landolt-Börnstein, Numerical Data and Functional Relationships in Science and Technology. New Series, Group III, 27/e. Berlin: Springer-Verlag; 1991.

[30] L. G. Van Uitert, E. M. Gyorgy, W. A. Bonner, W. H. Grodkiewicz, E. J. Heilner and G. J. Zydzik. Control of bubble domain properties in garnets. Mat. Res. Bull.. 1971;6:1185.

[31] M. Pashkevich, A. Stupakiewicz, A. Kirilyuk, A. Stognij, A. Maziewski, Th. Rasing. Magneto-optical spectroscopy of surface/interfaces in Co/garnet heterostructures. Appl. Surf. Sci.. 2014;305:117.

[32] S. Pal, B. Rana, O. Hellwig, T. Thomson and A. Barman. Tunable magnonic frequency and damping in $[Co/Pd]_8$ multilayers with variable Co layer thickness. Appl. Phys. Lett.. 2011;98:082501.

[33] S. Mizukami, E. P. Sajitha, D. Watanabe, F. Wu, T. Miyazaki, H. Naganuma, M. Oogane and Y. Ando. Gilbert damping in perpendicularly magnetized Pt/Co/Pt films investigated by all-optical pump-probe technique. Appl. Phys. Lett.. 2010;96:152502.

[34] J-M. L. Beaujour, J. H. Lee, A. D. Kent, K. Krycka and C-C. Kao. Magnetization damping in ultrathin polycrystalline Co films: Evidence for nonlocal effects. Phys. Rev. B. 2006;74:214405.

[35] M. Farle. Ferromagnetic resonance of ultrathin metallic layers. Rep. Prog. Phys.. 1998;61:755.

[36] H. Suhl. Ferromagnetic Resonance in Nickel Ferrite Between One and Two Kilomegacycles. Phys. Rev.. 1955;97:555.

[37] M. Maryško, J. Šimšová. Ferromagnetic resonance study of $Y_{3-z}\,Ca_{\,z}\,Fe_{5-x-y}\,Co_{\,x}\,Ge_{\,y}\,O_{12}$ films. Czech. J. Phys. B. 1984;34:1125.

[38] M. Maryško, P. Grnert and J. Pačes. Magnetic Properties of Cobalt-Doped YIG Films Compensated by Ge^{4+} and Ti^{4+}. Phys. Stat. Sol. A. 1991;123:303.

[39] G. Winkler. Magnetic Garnets. Braunschweig: Friedr. Vieweg & Sohn; 1981.

[40] M. Pashkevich, A. Stupakiewicz, A. Kirilyuk, A. Maziewski, A. Stognij, N. Novitskii, A. Kimel, Th. Rasing. Tunable magnetic properties in ultrathin Co/garnet heterostructures. J. Appl. Phys.. 2012;111:023913.

[41] A. Stupakiewicz, M. Pashkevich, A. Maziewski, A. Stognij, N. Novitskii. Spin precession modulation in a magnetic bilayer. Appl. Phys. Lett.. 2012;101:262406.

[42] M. Pashkevich, A. Stupakiewicz, A. Kimel, A. Kirilyuk, A. Stognij, N. Novitskii, A. Maziewski and Th. Rasing. Laser-induced magnetization dynamics in a cobalt/garnet heterostructure. Europhys. Lett.. 2014;105:27006.

[43] J.-Y. Bigot, M. Vomir, L. H. F. Andrade, E. Beaurepaire. Ultrafast magnetization dynamics in ferromagnetic cobalt: The role of the anisotropy. Chem. Phys.. 2005;318:137.

[44] M. Vomir, L. H. F. Andrade, L. Guidoni, E. Beaurepaire, and J.-Y. Bigot. Real Space Trajectory of the Ultrafast Magnetization Dynamics in Ferromagnetic Metals. Phys. Rev. Lett.. 2005;94:237601.

[45] J. Kisielewski, A. Kirilyuk, A. Stupakiewicz, A. Maziewski, A. Kimel, Th. Rasing, L.T. Baczewski, and A. Wawro. Laser-induced manipulation of magnetic anisotropy and magnetization precession in an ultrathin cobalt wedge. Phys. Rev. B. 2012;85:184429.